Using active colloids as machines to weave and braid on the micrometer scale

Carl P. Goodrich[a,b,1] and Michael P. Brenner[a,b]

[a]School of Engineering and Applied Sciences, Harvard University, Cambridge, MA 02138; and [b]Kavli Institute of Bionano Sciences and Technology, Harvard University, Cambridge, MA 02138

Edited by Tom C. Lubensky, University of Pennsylvania, Philadelphia, PA, and approved November 11, 2016 (received for review June 1, 2016)

Controlling motion at the microscopic scale is a fundamental goal in the development of biologically inspired systems. We show that the motion of active, self-propelled colloids can be sufficiently controlled for use as a tool to assemble complex structures such as braids and weaves out of microscopic filaments. Unlike typical self-assembly paradigms, these structures are held together by geometric constraints rather than adhesive bonds. The out-of-equilibrium assembly that we propose involves precisely controlling the 2D motion of active colloids so that their path has a nontrivial topology. We demonstrate with proof-of-principle Brownian dynamics simulations that, when the colloids are attached to long semiflexible filaments, this motion causes the filaments to braid. The ability of the active particles to provide sufficient force necessary to bend the filaments into a braid depends on a number of factors, including the self-propulsion mechanism, the properties of the filament, and the maximum curvature in the braid. Our work demonstrates that nonequilibrium assembly pathways can be designed using active particles.

colloidal machines | active colloids | self-assembly | braids and weaves

Biology has long been known to use a combination of programmable interactions with specific energy input through small molecules (ATP) to create remarkable machines. Because we have not yet developed the ability to emulate these machines artificially, understanding assembly pathways at the microscopic scale is a fundamental challenge in both biology and nanotechnology (1). However, recently there have been major advances in colloidal science, making it possible to program interactions between individual units. This has led to robust assembly of complex structures, approaching the complexity of biological systems. But biological systems also use specific energy input of small molecules to create machines. How can we do this with soft materials?

A parallel recent development has been to use chemical reactions on the surface of colloids to create motility mechanisms. This has led to the growth of the field of active matter, which aims to design, control, and understand self-propelled particles (2–12). These active particles provide significant yet untapped potential: by combining this mechanism for energy input with controllable interactions, it becomes possible to imagine the creation of colloidal-scale machines that can do work and perform tasks.

Here we present a proof-of-principle demonstration of how this could work. We show one way in which active colloids can be harnessed to drive the assembly of weaves and braids, turning long filaments into complex structures, using only active forces [e.g., hydrogen peroxide-propelled colloids (2–4)] and nonspecific short-range attractive forces (e.g., depletion forces). The typical self-assembly paradigm encodes information through the specific interactions between building blocks that in turn promote assembly. For example, a given amino acid sequence consistently folds into a specific protein structure, and DNA-coated colloids can be designed with specific interactions so that a desired structure is the thermodynamic ground state (13–15). Our approach differs in that the information for assembly is not coded directly into the building blocks but is instead encoded in the active colloids, which serve as a microscopic assembly machine.

With examples ranging from fabrics to ropes to wicker baskets, weaves and braids play a prominent technological role at the macroscopic scale. One advantage of weaves and braids is that they are held together by the topology of the constituent filaments, making such objects or materials highly stable. In addition, weaving and braiding can be an effective way to alter material properties. For example, the strength of rope comes from the friction of the braided threads, and power loss in current-carrying wires due to the skin effect and the proximity effect can be reduced by braiding multiple small wires together, making what is known as a Litz wire. However, although these advantages are particularly appealing at the microscopic scale, current technology does not include the ability to weave and braid microscopic filaments. [At the molecular scale, braids (16) and weaves (17) have been synthesized by chemically interlacing molecular building blocks, but this approach would clearly not work on the micrometer scale.]

Note that the topological constraints that make braids and weaves structurally stable also make self-assembly mechanisms for such small-scale structures challenging, because the structure cannot be assembled "all at once." It is necessary to start braiding at one end and work toward the other. Note that this feature distinguishes a braid from a twist, and we do not consider twists for the present work (although we will see how multiple twists can be combined to form a braid). We also do not consider knots, although it should be possible to extend our strategy to assemble such structures.

Our proposed scheme to weave and braid microscopic filaments with active particles is inspired by the so-called "maypole dance," which is depicted in the painting by Doris Lee shown in

Significance

Designing and building custom-made structures at the microscopic scale is a fundamental goal in nanotechnology. Many self-assembly approaches have the advantage of being autonomous in that no external input is required during the assembly process. We present a paradigm for the autonomous, out-of-equilibrium assembly of braids and weaves at the microscopic scale, using active particles. This approach, which involves controlling the precise motion of self-propelled colloids, not only provides a path for assembling complex structures but also demonstrates how active particles can be harnessed and used as a functional microscopic machine.

Author contributions: C.P.G. and M.P.B. designed research, performed research, analyzed data, and wrote the paper.

The authors declare no conflict of interest.

This article is a PNAS Direct Submission.

[1]To whom correspondence should be addressed. Email: goodrich@g.harvard.edu.

This article contains supporting information online at www.pnas.org/lookup/suppl/doi:10.1073/pnas.1608838114/-/DCSupplemental.

Fig. 1. "Schoolyard Maypole Dance," by Doris Lee, May 4, 1946. In a maypole dance, motion in 2D leads to a braided structure. By controlling the precise motion of colloids that are attached to long filaments, this concept can be translated to the micrometer scale. *Maypole Dance* illustration courtesy of ©SEPS licensed by Curtis Licensing, Indianapolis, IN.

Fig. 1. To perform this dance, a number of ribbons are attached at one end to the top of a large pole and held at the other end by the dancers. Moving in opposite directions, some clockwise and some counterclockwise, the dancers weave in and out of each other, pulling their ribbons with them. Importantly, the dancers' collective paths have a nontrivial topology, which is reflected in the woven structure of the filaments at the top of the painting. Note that the pole itself is necessary only to keep the top ends of the ribbons attached together and suspended.

The maypole dance demonstrates how motion in two dimensions can assemble a complex 3D structure, a basic principle behind modern industrial braiding machines. Our strategy uses this idea at the microscopic scale by using active colloids instead of human dancers. If the 2D motion of the colloids can be precisely controlled, then attaching filaments to the colloids would result in the filaments weaving together according to the motion of the colloids. The challenge clearly becomes controlling the precise motion of the colloids necessary for the desired structure.

Assembly via Active Colloids

How can one control the 2D motion of colloids? One approach, demonstrated by Pieranski et al. (18), is to control particle motion externally through, for example, a magnetic field. However, this does not provide much flexibility and we seek a scheme that, similar to many self-assembly approaches, does not rely on any external control. Active, self-propelled particles offer an intriguing alternative. In addition to thermal motion, an active colloid on its own moves in a specific direction, which changes over time due to angular diffusion. Therefore, any attempt to control the motion of active colloids must be able to influence their orientations, and the simplest way to do this is to design some sort of track for the particles to move in. One possibility would be to use photolithography to create an indented track that guides an active rod-shaped particle via steric interactions. Another one, which we discuss below, is to use photolithographic micropillars and short-range attractive forces to guide two spherical colloids. Although slightly more complicated, this approach is more interesting and offers more flexibility.

Consider three colloids of equal radius confined to 2D and arranged in a triangle, as shown at the right of Fig. 2*A*. The blue "fixed" particle cannot move and in practice could be a micropillar created by photolithography rather than a colloid, while the red "active" particle moves in the direction of the orange "passive" particle. There are various possibilities for implementing this type of active force experimentally (for example, using the asymmetric dimers of ref. 19 or even the "lock and key" scheme of ref. 20), but for our purposes we simply take this as a given rule. In addition, all colloids experience steric repulsions and a very short-range attractive force, for example from depletion interactions.

For a system of just the micropillar and two colloids, the active colloid pushes the passive colloid in a clockwise circle around the micropillar. (This assumes that the active force is large enough to overcome friction and small enough to prevent the colloids from detaching from the micropillar.) Now consider placing a second micropillar at a distance from the first micropillar such that the colloids fit snugly between them. When the passive particle passes between the two micropillars, the attractive depletion forces cancel. Importantly, the force from the active particle is at an angle (position "2" in Fig. 2*A*) so that the passive particle is

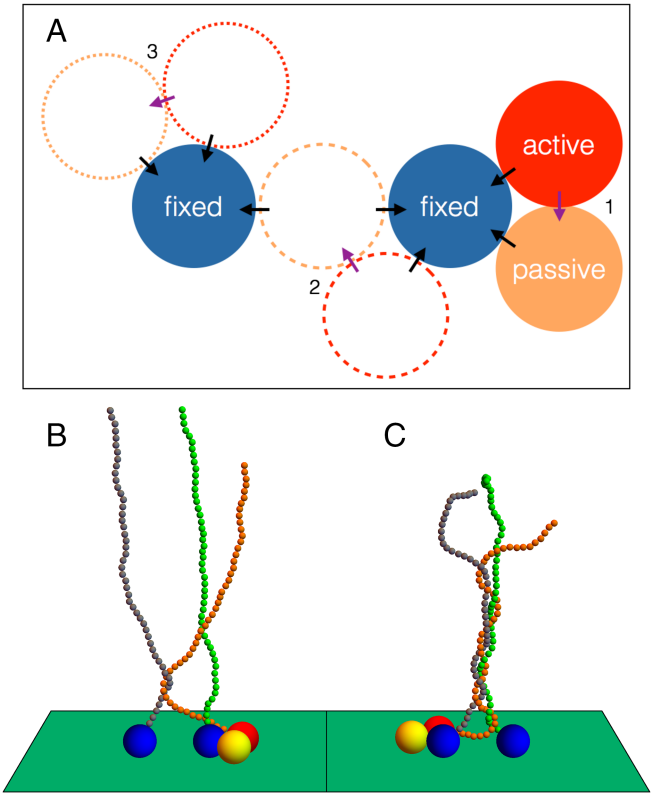

Fig. 2. Assembling a simple braid. (*A*) Two-dimensional schematic of figure-eight motion. An active (red) and a passive (orange) colloid can be designed to perform a figure-eight motion around two fixed micropillars (blue), as discussed in the text. The active particle is designed to push into the passive particle, as shown by the purple arrows. The black arrows show the depletion forces with the micropillars. (*B* and *C*) Brownian dynamics simulation of three filaments being braided by the figure-eight motion of the active colloid, with snapshots taken after approximately 1 full period (*B*) and 3.5 full periods (*C*) of the figure-eight motion. The full simulation can be seen in Movie S1.

pushed completely onto the second micropillar. (This assumes that the active force is strong enough to overcome the energy barrier associated with binding between the passive particle and the first micropillar.) The same happens for the active particle, and the active–passive pair proceeds on to position "3." The pair then circles counterclockwise around the second micropillar before jumping back to the first micropillar to complete a "figure eight."

This motion now can be exploited to form a braid by attaching filaments to the two micropillars and the active particle. [Binding the third filament to the passive particle rather than to the active particle makes the system more susceptible to "mistakes" at position 2 when trying to cross from one micropillar to the other (discussion below).] As a proof-of-principle demonstration, we run Brownian dynamics simulations of the micropillars, colloids, and attached filaments, as discussed in more detail in *Materials and Methods*. Our model is intentionally simplistic because we want to focus on the general idea of braiding with active colloids and not limit ourselves to any one specific implementation. We discuss limits of experimental feasibility below. Fig. 2*B* shows the system in position "1" after one full period of the motion. The active colloid and micropillars are attached to filaments composed of 50 monomers each that were placed initially in a vertical line. Fig. 2*B* clearly shows how the orange filament (attached to the active colloid) wraps around and between the other two filaments. The braided structure is apparent in Fig. 2*C*, which shows the system in position 3 after 3.5 periods.

Note that the figure-eight motion is achieved using only ingredients that are individually well studied: active particles, depletion forces (or some other short-range attraction), and photolithography to set the precise geometry of the fixed micropillars. In addition, note that the structure of the braid is not affected if the path of the colloids is smoothly deformed provided that the deformation does not move the path through one of the micropillars. However, a path that, for example, circled only one of the micropillars without ever going around the other would produce a distinctly different braid. Thus, the braid structure can be described in terms of the topology of the path of the colloids on a 2D plane with the micropillars cut out.

Finally, note that the braid starts at the bottom and propagates up the filaments over time. In our example simulation, the top ends of the filaments are free and thus the braid unravels when it reaches the top. This can be prevented in a number of ways, for example by fixing the top ends together or attaching them to some other object (similar to the top of the pole in the maypole dance). The upward propagation of the braid depends on a number of factors, including the forces applied by the colloids at the bottom, the stiffness of the filaments, and the friction associated with filaments sliding past each other. In the maypole dance, the braid does not propagate but instead starts at the top because tension is maintained in the ribbons throughout the dance. In principle, the braiding of the filaments could also start at the top end if tension could be maintained throughout.

An alternate approach, which we demonstrate in our second example of active assembly, is to take advantage of the friction between filaments. In industrial weaving and braiding machines, the threads do not slide past each other; instead, new thread is continuously fed in at the braiding end. This corresponds to designing the filaments to grow at the end where they attach to the colloids. Although it may be difficult to design a specific filament to polymerize at an end that is also bound, we note that such behavior is not impossible and has been observed in cross-linked actin filaments (21–23).

The simulation shown in Fig. 3 demonstrates two important extensions of the scheme shown in Fig. 2. First, the figure-eight motion can be used as a building block to design more complicated topological motion and thus more intricate structures. Fig. 3*A* shows a line of five micropillars instead of just two; the active and passive colloids weave in and out of the micropillars, as shown. Second, the filament attached to the active colloid grows as the particles move.

When attached to filaments, the motion shown in Fig. 3*A* results in a more traditional weave structure with five "warp" strands (shown in gray in Fig. 3 *B* and *C*) and one "weft" strand (shown in green in Fig. 3 *B* and *C*). In our Brownian dynamics simulations, we allow the green weft strand to polymerize at the end that is attached to the active particle (see *Materials and Methods* for more details). Matching the polymerization rate approximately to the lateral speed of the active particle prevents the weft strand from constantly being pulled through the structure and allows one to build larger structures. [In our simulations the polymerization rate is set by the concentration of diffusing monomers, which can easily be adjusted. In experimental systems, the ability to control the polymerization rate depends on the details of the system. In some cases, it is possible that force-sensitive polymerization could stabilize this process (24).] In Fig. 3*C*, the weave pattern is clearly visible.

Fig. 4 shows a final and slightly different example of assembling a braid using active particles. The setup is fairly simple: Two sets of active–passive colloids are set up to circle clockwise around separate micropillars. Unlike the above examples, the colloids do not jump from one micropillar to the other because the micropillars are sufficiently separated. When filaments are

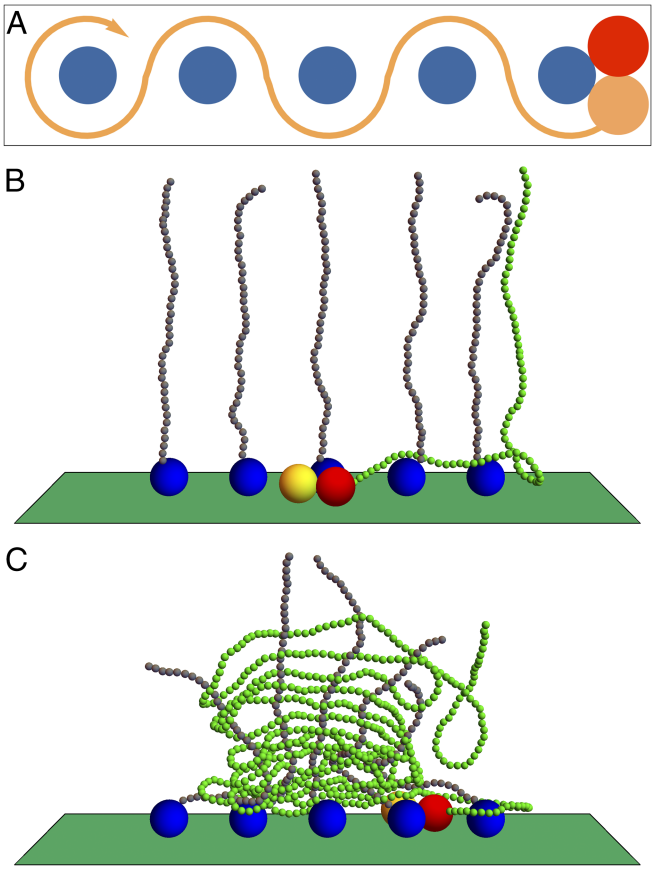

Fig. 3. Assembling a six-strand weave. (*A*) Diagram of the 2D motion of the colloids. (*B*) Five warp filaments (gray) are attached to the fixed colloids and a single weft filament (green) is attached to the active colloid. A bath of free monomers (not shown for clarity) can polymerize the end of the weft filament, causing it to grow as it is pulled between the micropillars. (*C*) After eight full periods of the motion, the weave pattern is clearly visible. The full simulation can be seen in Movie S2.

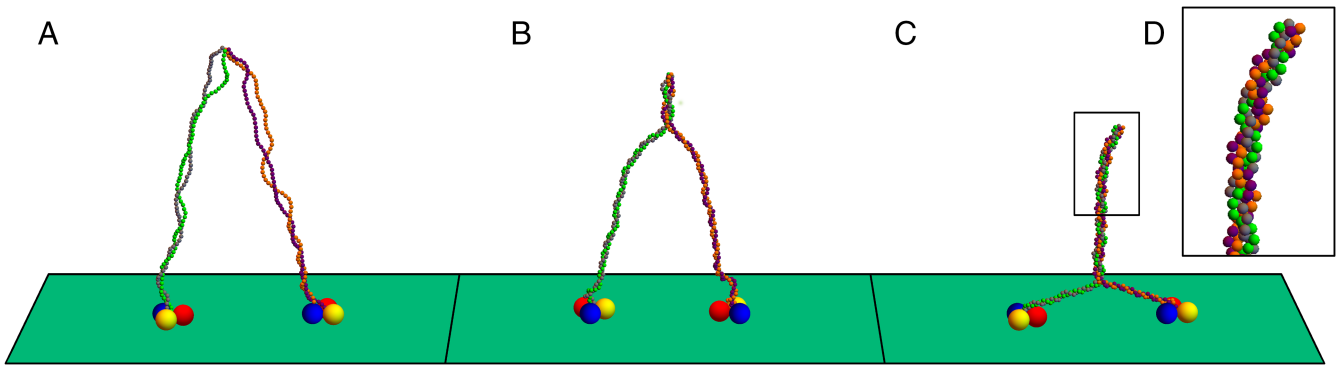

Fig. 4. Inducing a twist braid. (*A*) Active/passive colloids rotate clockwise around two fixed colloids, causing right-handed twists in the attached filaments. (*B*) The four filaments are connected at the top end and cannot untwist, but some tension can be relieved through a secondary left-handed twist of the two filament pairs. (*C*) This secondary twist propagates downward and can reach the base of the system. (*D*) A close-up of the final twist-braid structure from *C*. The full simulation can be seen in Movie S3.

attached (again to the active colloids and micropillars), this causes the filament pairs to twist (Fig. 4*A*). Now, attaching the four filaments together at the opposite end prevents the filaments from unraveling. As the twists propagate up the filaments, a torque develops at the top because both filament pairs want to twist in the same direction. This leads to a secondary twist in the opposite direction to relieve the tension, which can be seen in Fig. 4*B*. As the initial twists tighten, this secondary twist propagates down the length of the system (Fig. 4*C*). A close-up of the final twist braid is shown in Fig. 4*D*.

This scheme is significantly simpler than the previous examples because the active colloids simply rotate about the micropillars, and there are many ways to get colloids to actively rotate (7, 25–29). Despite the simplicity of the motion of the individual active particles, the combination is sufficient to create a braid, further demonstrating the robustness of active particles as an assembly machine. In addition, the simulation in Fig. 4 shows two groups of two filaments each, but each group can have an arbitrary number of filaments and there can also be more than just two groups. The high symmetry of twist braids makes them ideal for many applications, ranging from rope and string to Litz wires.

For these schemes to successfully produce braids, the active colloids must be able to generate sufficient forces to bend the filaments. In *Supporting Information*, we approximate the force necessary to bend various biopolymers (30) into a braid and compare this with the potential driving force of a commonly studied active colloid (31) (Fig. S1). Whether the driving force is sufficient depends sensitively on the details of the application (in some cases it should work and in some cases it will not), and the technological challenge of increasing the driving force of active particles in order to broaden the applicability of these schemes warrants further investigation.

Better Ways to Control Colloidal Motion

The topology of the motion shown in Figs. 2 and 3 relies on the passive particle successfully jumping from one micropillar to another when it is in position 2 in Fig. 2*A*. This happens because the force from the active particle pushes the passive particle in the correct direction. However, the passive particle can sometimes "make a mistake" due to thermal fluctuations and remain with the original micropillar. The frequency of such mistakes depends not only on the temperature of the system but also on the precise form of the interactions and the geometry of the micropillars (see *Materials and Methods* for details of our simulations).

Because any investigation of the frequency of mistakes would be applicable only to our somewhat crude model, we instead present an alternate scheme to get the particle to jump from one micropillar to another. This alternate scheme, depicted in Fig. 5 *A* and *B*, is not susceptible to such mistakes and is perhaps more feasible experimentally. Note that using photolithography to grow the fixed micropillars has the advantage that the position and size of the micropillars can be controlled precisely. In addition, photolithographic micropillars can be grown in any desired shape to high precision.

Consider two micropillars, shown in blue in Fig. 5*A*, that instead of being circularly shaped as in Fig. 2*A* come to a point (Fig. 5*B* shows a close-up view). Now, instead of an active colloid and a passive colloid that are designed such that the active force always points in the direction of the passive particle, consider a single rod-shaped colloid with one active end, as shown. When in position 1 in Fig. 5*B*, depletion forces keep the rod pressed against the flat side of the micropillar so the motion is tangential to the surface even if the micropillar curves slightly. However, if the side of the micropillar ends abruptly, the active rod will move off the micropillar. The key is for the second micropillar to "catch" the rod, as shown in position 2 in Fig. 5*B*. This requires that the rod be long enough so that its orientation is always controlled by the depletion forces associated with one of the micropillars and also that the spacing of the micropillars be engineered to match the width of the rod. Fig. 5 *A* and *B* shows an active rod jumping from one micropillar to another as it moves from the bottom right to the top left. Clearly, a rod moving up and to the right from the bottom left would also successfully jump from one micropillar to the other. This is the key feature necessary for the braiding and weaving in Figs. 2 and 3.

Note that the precise shape of the rest of the micropillar does not matter as long as the curvature is small enough that the rod does not spontaneously detach. Therefore, just as the figure-eight motion in Fig. 2 was extended to obtain the weave of Fig. 3, the scheme in Fig. 5*B* is also a building block that can lead to more complicated motion. For example, the eye-shaped micropillars in Fig. 5*C* lead to the same weave motion as in Fig. 3. Furthermore, such a line of micropillars can bend sharply or even circle onto itself, leading to a cylindrical weave structure (i.e., a sleeve).

Instead of using depletion forces (or some other short-range attractive force) to keep the rod tethered to the micropillars, there could also be a large micropillar encompassing the path so that the active rod simply moves along a track. The use of depletion forces has the effect of allowing a track to be "one sided," which may make it easier for freely moving active colloids to attach themselves to the track. We stress that the possible strategies for designing such a track are not limited to those presented here.

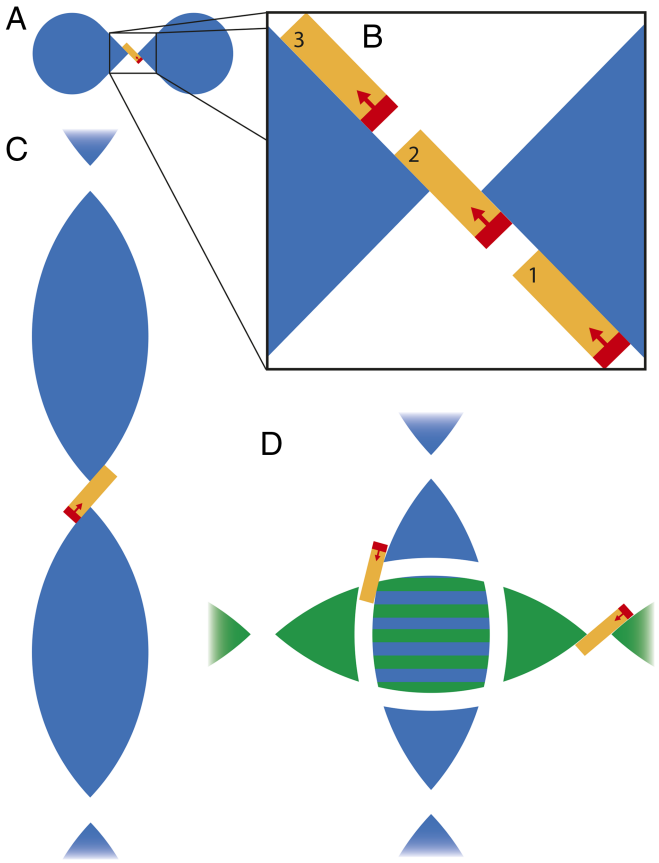

Fig. 5. Building blocks for the active assembly of complex structures. (*A*) An alternate approach to the figure-eight motion. Two circular photolithographic micropillars come to a point facing each other. With the extreme flexibility and robustness of photolithography, micropillars can be fabricated in any shape to high precision. This geometry allows a rod-shaped active colloid that is attracted to the micropillars through depletion forces to perform a figure-eight motion. (*B*) A close-up showing the transfer in *A* of the active colloid from one micropillar to the other. The rod starts in position 1 and moves up and to the left. In position 2, the colloid has partially moved off the right micropillar and is held in place by both the left and right micropillars. In position 3, the colloid has completely transferred to the left micropillar. Due to the symmetry in the geometry of the micropillars, a colloid coming from the bottom left would transfer to the top right. (*C*) This scheme can be extended (in analogy to Fig. 3) by using a series of eye-shaped micropillars. The fading at the top and bottom indicates that the micropillars extend beyond what is shown. The series of eye-shaped micropillars can be terminated by a circular micropillar similar to what is shown in *A*. (*D*) Example of a more complicated micropillar track composed of a vertical track (blue) similar to *C* and a crossing horizontal track (green). Holes in the intersecting micropillar allow colloids to pass through unaffected.

Finally, we are now in a position to introduce a more intricate building block that was not possible using the cylindrical micropillars. Fig. 5*D* shows a vertical line of eye-shaped micropillars similar to Fig. 5*C* (blue) as well as a horizontal line of eye-shaped micropillars (green). Note that the central intersecting micropillars have gaps in them that allow for the rods to pass through them. For example, the active rod traveling from top to bottom along the blue vertical micropillars can pass over the gap (as shown) and continue unaffected along the blue micropillars. Similarly, an active rod moving from right to left along the green horizontal micropillars can pass through the vertical blue micropillars. Combined with the fact that the lines of micropillars can bend, loop, and terminate, this additional building block allows for the possible construction of much more complex and interesting structures beyond classical braids and weaves.

Conclusion

We have demonstrated that nonequilibrium assembly pathways can be designed using active particles, which serve as autonomous and programmable microscopic machines. This result leads to an approach to microassembly where complex objects composed of semiflexible filaments are constructed using active colloids; this paradigm is highly robust, extendable, and scalable. Unlike most nonequilibrium biological processes, our mechanism does not rely on ATP for a fuel source. Instead, it uses a controllable chemical reaction, for example, to generate motion, which suggests a possible alternative to complex ATP-driven machinery in the development of artificial microscopic machines.

Our assembly mechanism itself uses self-propelled colloids that, in analogy to the maypole dance, move in a path with a specific topology and thereby pull filaments into a braid or weave. This converts the assembly problem into a matter of controlling the motion of the active colloids. We have presented a few schemes for achieving this without any external input, accompanied by proof-of-principle Brownian dynamics simulations (Figs. 2–4). In particular, the micropillar geometry shown in Fig. 5 should be both experimentally relevant and also highly robust and extendable, allowing for the assembly of increasingly complex structures. However, we emphasize that there are many other possible schemes to achieve motion with a specific topology that may be more relevant to different applications, and the notion of active assembly is by no means limited to the schemes presented here.

Materials and Methods

Interactions. We perform Brownian dynamics simulations to demonstrate how the 2D motion of active colloids can braid and weave filaments. The colloids are modeled as spheres of radius R_L whereas the filaments are chains of monomers (discussed below) that are modeled as spheres of radius $R_S = R_L/5$. The micropillars are treated as colloids whose position is fixed. When any two spheres overlap, they feel a simple harmonic repulsive interaction of the form

$$U_H(r) = \frac{1}{2}k_H(r-\sigma)^2\Theta(\sigma - r), \quad [1]$$

where $\Theta(x)$ is the Heaviside step function and σ is the sum of the radii of the two spheres.

For simplicity, the large colloids are restricted to move in a horizontal plane at the bottom of the system. In an experimental system, depletion forces could be used to keep the colloids attached to a horizontal plate. We model the short-range attractive forces between the large colloids using a generic one-sided cutoff Morse potential of the form

$$U_M(r) = k_{M,0}\left(\frac{\left(1-e^{-a(r-r_0)}\right)^2}{2a^2} + C + Dr\right)\Theta(r-\sigma)\,\Theta(R_{\text{off}} - r), \quad [2]$$

where

$$a = a_0/\sigma, \quad [3]$$

$$R_{\text{off}} = (1 + 4/a_0)\sigma, \quad [4]$$

$$r_0 = \frac{1}{a}\log\left(\frac{e^{a(\sigma+R_{\text{off}})}}{e^{a\sigma}+e^{aR_{\text{off}}}}\right), \quad [5]$$

$$k_{M,0} = \frac{k_M\left(e^{a\sigma}+e^{aR_{\text{off}}}\right)^2}{e^{2aR_{\text{off}}} - e^{a(\sigma+R_{\text{off}})}}. \quad [6]$$

R_{off} is a cutoff distance and the constants C and D are set so that $U_M(r)$ and its derivative continuously approach zero at R_{off}. Thus, for given values of a_0 and k_M, we have $\frac{dU_M}{dr}(R_{\text{off}}) = \frac{dU_M}{dr}(\sigma) = 0$, and $\frac{d2U_M}{dr2}(\sigma) = k_M$. Finally, the active colloid experiences a force of magnitude f_A in the direction of the passive particle. Because the passive particle does not experience an equal and opposite force, this cannot be written as the gradient of an energy surface and injects energy into the system.

The centers of the micropillars in Figs. 2 and 3 should be separated by approximately $4R_L$ so that the active and passive colloids just fit between. Given the shape of the Morse potential, we choose the actual separation

to be $4.15R_L$. This flattens slightly the energy landscape of the active and passive particles between the two micropillars, but we stress that this is not essential to the success of the scheme. If an experimental system uses hard colloids, some amount of leeway of this sort will of course be necessary.

The filaments are modeled as chains of the small monomers of radius R_S. For two neighboring monomers in a chain, the Heaviside function in Eq. **1** is simply removed so the monomers are connected by a two-sided spring. In addition, filaments exhibit a bond-bending stiffness. For consecutive monomers *h*, *i*, and *j* in a filament, the bond-bending energy takes the form

$$U_{BB}\left(\theta_{hij}\right) = \frac{1}{2}k_{BB}\left(\cos\theta_{hij} - 1\right)^2, \qquad [7]$$

where θ_{hij} is the angle formed by the bond between monomers *h* and *i* and the bond between monomers *i* and *j* (note that $\theta_{hij} = 0$ when the particles are colinear). We note that this model is quantitatively very similar to one used to model actin filaments (23). Finally, one end of each filament is attached to one of the large colloids or micropillars by a two-sided spring, which again is implemented by simply removing the Heaviside function from Eq. **1**.

We note that we do not directly include hydrodynamic interactions between the filaments, which could affect the unraveling of a braid or weave at a free end. However, this would not change the qualitative results of Figs. 2–4 and there is a history of Brownian dynamics well capturing the relaxation of polymers (32–36). In addition, we neglect lubrication forces, which in principle could affect the moment when the active and passive colloids move from one fixed micropillar to the other but in practice will have a negligible effect due to surface roughness.

Dynamics. The overdamped Langevin equation for particle *i* is

$$\frac{d\mathbf{r}_i}{dt} = \frac{1}{\gamma_i}\mathbf{F}_i + \sqrt{\frac{2k_BT}{\gamma_i}}\mathbf{f}_i(t), \qquad [8]$$

where γ_i is a friction coefficient, $\mathbf{F}_i$ is the total force on the particle (i.e., the sum of the forces outlined above), and the elements of $\mathbf{f}_i(t)$ are Gaussian random variables that satisfy $\langle f_i^\alpha(t)\rangle = 0$ and $\left\langle f_i^\alpha(t)f_j^\beta(t')\right\rangle = \delta_{i,j}\delta_{\alpha,\beta}\delta(t-t')$, where α and β index spatial dimensions. For spherical particles of radius R_i, the friction coefficient is $\gamma_i = 2d\pi\eta R_i$, where η is the dynamic viscosity of the system. The diffusion coefficient of the particle is

$$D_i = \frac{k_BT}{\gamma_i} = \frac{k_BT}{2d\pi\eta R_i}. \qquad [9]$$

Eq. **8** is simulated using a time step of $\Delta t = 10^{-3}$, which is much slower than the relevant dynamics in the system.

Polymerization. The simulation in Fig. 3 includes polymerization of the green filament at the end attached to the active colloid. This was implemented by including 1,500 free monomers (spheres of radius R_S) that diffuse throughout the periodic box (which has dimensions $150R_S \times 50R_S \times 100R_S$) and are not shown in the images in Fig. 3 for clarity. When a free monomer comes into contact with the head of the green filament (meaning the end monomer that is attached to the active colloid), the free monomer is added onto the green filament and becomes the new head. Note that the small discontinuities in force caused by this abrupt polymerization are too small to affect the overall dynamics of the system.

For the parameters in our model, we use the following values: $R_S = 1$, $R_L = 5$, $k_H = 200$, $k_M = 400$, $k_{BB} = 200$, $a_0 = 18$, $f_A = 40$, $\eta = 1$, $k_BT = 1$, and $\Delta t = 10^{-3}$.

ACKNOWLEDGMENTS. We thank Amy Duwel, Viva Horowitz, Vinothan Manoharan, Sabetta Matsumoto, and Mohammad Shahjamali for helpful discussions. This research was funded by the National Science Foundation through the Harvard Materials Research Science and Engineering Center Grant DMR1420570 and the Division of Mathematical Sciences Grant DMS-1411694 and also by the Air Force Research Laboratory and the Defense Advanced Research Agency through a subcontract from The Charles Stark Draper Laboratory. M.P.B. is an investigator of the Simons Foundation.

1. Whitesides GM, Grzybowski B (2002) Self-assembly at all scales. *Science* 295(5564): 2418–2421.
2. Paxton WF, et al. (2004) Catalytic nanomotors: Autonomous movement of striped nanorods. *J Am Chem Soc* 126(41):13424–13431.
3. Golestanian R, Liverpool TB, Ajdari A (2005) Propulsion of a molecular machine by asymmetric distribution of reaction products. *Phys Rev Lett* 94(22):220801–220804.
4. Howse JR, et al. (2007) Self-motile colloidal particles: From directed propulsion to random walk. *Phys Rev Lett* 99(4):048102–048104.
5. Ramaswamy S (2010) The mechanics and statistics of active matter. *Annu Rev Condens Matter Phys* 1(1):323–345.
6. Liu R, Sen A (2011) Autonomous nanomotor based on copper–platinum segmented nanobattery. *J Am Chem Soc* 133(50):20064–20067.
7. Schwarz-Linek J, et al. (2012) Phase separation and rotor self-assembly in active particle suspensions. *Proc Natl Acad Sci USA* 109(11):4052–4057.
8. Fily Y, Marchetti MC (2012) Athermal phase separation of self-propelled particles with no alignment. *Phys Rev Lett* 108(23):235702.
9. Marchetti MC, et al. (2013) Hydrodynamics of soft active matter. *Rev Mod Phys* 85(3):1143–1189.
10. Palacci J, Sacanna S, Steinberg AP, Pine DJ, Chaikin PM (2013) Living crystals of light-activated colloidal surfers. *Science* 339(6122):936–940.
11. Palacci J, et al. (2014) Light-activated self-propelled colloids. *Philos Trans A Math Phys Eng Sci* 372(2029):20130372.
12. Stenhammar J, Wittkowski R, Marenduzzo D, Cates ME (2016) Light-induced self-assembly of active rectification devices. *Sci Adv* 2(4):e1501850.
13. Hormoz S, Brenner MP (2011) Design principles for self-assembly with short-range interactions. *Proc Natl Acad Sci USA* 108(13):5193–5198.
14. Zeravcic Z, Manoharan VN, Brenner MP (2014) Size limits of self-assembled colloidal structures made using specific interactions. *Proc Natl Acad Sci USA* 111(45): 15918–15923.
15. Rogers WB, Manoharan VN (2015) Programming colloidal phase transitions with DNA strand displacement. *Science* 347(6222):639–642.
16. Luo F, et al. (2011) New topology observed in highly rare interlaced triple-stranded molecular braid. *CrystEngComm* 13(2):421–425.
17. Liu Y, et al. (2016) Weaving of organic threads into a crystalline covalent organic framework. *Science* 351(6271):365–369.
18. Pieranski P, Clausen S, Helgesen G, Skjeltorp AT (1996) Braids plaited by magnetic holes. *Phys Rev Lett* 77(8):1620–1623.
19. Ma F, Yang X, Zhao H, Wu N (2015) Inducing propulsion of colloidal dimers by breaking the symmetry in electrohydrodynamic flow. *Phys Rev Lett* 115(20):208302–208305.
20. Sacanna S, Irvine WTM, Chaikin PM, Pine DJ (2010) Lock and key colloids. *Nature* 464(7288):575–578.
21. Lasa I, et al. (1997) Identification of two regions in the N-terminal domain of ActA involved in the actin comet tail formation by Listeria monocytogenes. *EMBO J* 16(7):1531–1540.
22. Egile C, et al. (1999) Activation of the CDC42 effector N-WASP by the Shigella flexneri IcsA protein promotes actin nucleation by Arp2/3 complex and bacterial actin-based motility. *J Cell Biol* 146(6):1319–1332.
23. Banigan EJ, Lee KC, Liu AJ (2013) Control of actin-based motility through localized actin binding. *Phys Biol* 10(6):066004–066014.
24. Dickinson RB (2008) Models for actin polymerization motors. *J Math Biol* 58(1-2):81–103.
25. Grzybowski BA, Stone HA, Whitesides GM (2002) Dynamics of self assembly of magnetized disks rotating at the liquid-air interface. *Proc Natl Acad Sci USA* 99(7):4147–4151.
26. Catchmark JM, Subramanian S, Sen A (2005) Directed rotational motion of microscale objects using interfacial tension gradients continually generated via catalytic reactions. *Small* 1(2):202–206.
27. Riedel IH, Kruse K, Howard J (2005) A self-organized vortex array of hydrodynamically entrained sperm cells. *Science* 309(5732):300–303.
28. Dhar P, et al. (2006) Autonomously moving nanorods at a viscous interface. *Nano Lett* 6(1):66–72.
29. Wykes MSD, et al. (2016) Dynamic self-assembly of microscale rotors and swimmers. *Soft Matter* 12(20):4584–4589.
30. Broedersz CP, MacKintosh FC (2014) Modeling semiflexible polymer networks. *Rev Mod Phys* 86(3):995–1036.
31. Ebbens S, Tu MH, Howse JR, Golestanian R (2012) Size dependence of the propulsion velocity for catalytic Janus-sphere swimmers. *Phys Rev E Stat Nonlin Soft Matter Phys* 85(2 Pt 1):020401–020404.
32. Shaqfeh ESG (2005) The dynamics of single-molecule DNA in flow. *J Nonnewton Fluid Mech* 130(1):1–28.
33. Doyle PS, Ladoux B, Viovy JL (2000) Dynamics of a tethered polymer in shear flow. *Phys Rev Lett* 84(20):4769–4772.
34. Doyle PS, Shaqfeh ESG, GAST AP (1997) Dynamic simulation of freely draining flexible polymers in steady linear flows. *J Fluid Mech* 334:251–291.
35. Chopra M, Larson RG (2002) Brownian dynamics simulations of isolated polymer molecules in shear flow near adsorbing and nonadsorbing surfaces. *J Rheol* 46(4):831–833.
36. Ladoux B, Doyle PS (2000) Stretching tethered DNA chains in shear flow. *Europhys Lett* 52(5):511–517.
37. Baraban L, et al. (2012) Transport of cargo by catalytic Janus micro-motors. *Soft Matter* 8(1):48–52.
38. Howard J (2001) *Mechanics of Motor Proteins and the Cytoskeleton* (Sinauer Associates, Inc., Sunderland, MA).

Supporting Information

Goodrich and Brenner 10.1073/pnas.1608838114

Can Active Particles Provide Enough Force to Braid?

Here we consider the question of whether an active colloid is capable of providing enough force to bend a semiflexible filament enough to braid it. This is a difficult question to answer generically because the constraints will vary wildly depending on the application—relevant considerations include the bending rigidity, diameter, and maximum contour length of the filament or biopolymer; the type of braid/weave; the pitch; the number of periods; and the active mechanism for self-propulsion. Nevertheless, we proceed by approximating the force needed to bend various biopolymers and comparing this to the driving force of commonly used active particles.

Note that catalytic micromotors are able to provide forces sufficient for cargo transport (37), demonstrating that they are able to move more than just themselves. The actual amount of force that an active particle can generate depends on the mechanism for self-propulsion and the details of the particle, but we can make a rough estimate by considering the polystyrene microspheres of Ebbens et al. (31) that are half-coated in platinum. The platinum reacts with hydrogen peroxide to create a concentration gradient across the particle that propels the particle forward. Ebbens et al. measured particle velocities of approximately $2\,\mu$m/s, which corresponds to a drag force of approximately 2×10^{-13} N (given the reported diameter of $5\,\mu$m). This gives an estimate for the potential driving force of the particle.

Because curvature changes throughout the braid (Figs. 2 and 3), we consider the simpler case of a filament coiled into a helix with radius R_m and pitch p. In a helix, the radius of curvature, R_c, is constant along the filament and is given by

$$\frac{1}{R_\mathrm{c}}=\frac{4\pi^2R_\mathrm{m}}{p^2+4\pi^2R_\mathrm{m}^2}. \qquad \textbf{[S1]}$$

To calculate the force necessary to induce this amount of curvature, we treat the end of the filament as a cantilevered beam (38). Consider a straight filament of length L_end that lies along the x axis and is clamped at one end. We take this end to be the origin, so the clamping constrains the position of the filament and its derivative to satisfy $y(0)=y'(0)=0$. The colloid, which is attached at the other end, applies a perpendicular force F at $x=L_\mathrm{end}$. When this perpendicular force is small, the filament deflects and takes a shape given by $y(x)=(F/\kappa)\left(L_\mathrm{end}x^2/2-x^3/6\right)$, where κ is the bending stiffness of the filament (38). At $x=0$ the radius of curvature is $R_c(x=0)=\kappa/FL_\mathrm{end}$. If we make the reasonable approximation that L_end should be roughly given by the pitch, $L_\mathrm{end}\approx p$, we can approximate the force needed to bend the filament as

$$F=\frac{4\pi^2\kappa R_m}{p\left(p^2+4\pi^2R_m^2\right)}=\frac{\kappa\cos^2\lambda\cot\lambda}{2\pi R_m^2}, \qquad \textbf{[S2]}$$

where $\lambda\equiv\tan^{-1}\left(p/2\pi R_m\right)$ is the pitch angle and can be in the range $0\le\lambda\le\pi/2$. Note that $\kappa=k_\mathrm{B}TL_\mathrm{p}$, where L_p is the persistence length of the filament at temperature T.

In this calculation, we assume that the filament is relatively straight, meaning that the contour length of the filament, L, should be less than roughly the persistence length ($L\le L_\mathrm{p}$). In addition, real filaments cannot be arbitrarily long and have a natural bound on their contour length ($L\le L_\mathrm{max}$). The contour length in turn sets an approximate upper bound on the pitch ($p\le L$) because we want the filament to bend by a nonnegligible amount relative to the length. Thus, we want to know the force from Eq. **S2** for values of p/L less than 1.

To calculate the force necessary to braid real filaments, we use the data in table 1 in ref. 30 for the approximate diameter, persistence length, and maximum contour length of various biopolymers (microtubule, F-actin, intermediate filaments, and DNA) as well as SWNTs. We set the filament length to $L=\min(L_\mathrm{p},L_\mathrm{max})$ and let the pitch be in the range $0\le p\le L$. Fig. S1 shows the force from Eq. **S2** as a function of p/L, where we have taken R_m to be twice the filament diameter. At the beginning of the assembly process, the pitch can be as large as the contour length ($p/L=1$), but as the braid forms the maximum pitch necessarily decreases. By comparing these curves to the 2×10^{-13} N that we estimated above for the approximate driving force of active particles (dashed line), we get an estimate for the minimum pitch that can be achieved using active colloids. Whether this is sufficient depends of course on the application, but it is clear that the driving force of active particles will be the limiting variable for many systems. However, the driving force could presumably be increased by, for example, increasing the concentration of the fuel molecules (31).

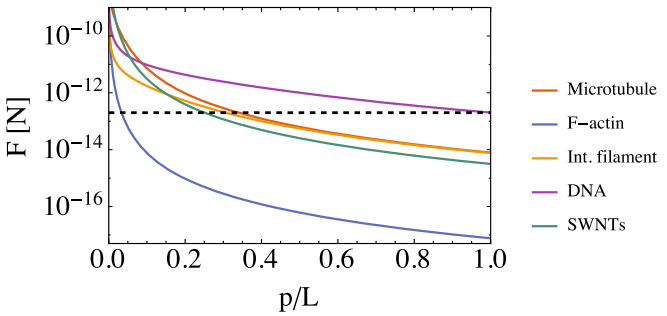

Fig. S1. Estimate of the bending force as a function of pitch divided by the filament length. Curves are shown for microtubule, F-actin, intermediate filaments (Int. filament), DNA, and single-walled carbon nanotubes (SWNTs). The persistence length (1 mm, 17 μm, 0.6 μm, 50 nm, and 10μm, respectively), approximate diameter (25 nm, 7 nm, 9 nm, 2 nm, and 1 nm, respectively), and maximum contour length (10 μm, 20 μm, 6 μm, 1 m, and 1 μm, respectively) were taken from ref. 30. The dashed line shows the driving force of 2×10^{-13} N extracted from ref. 31.

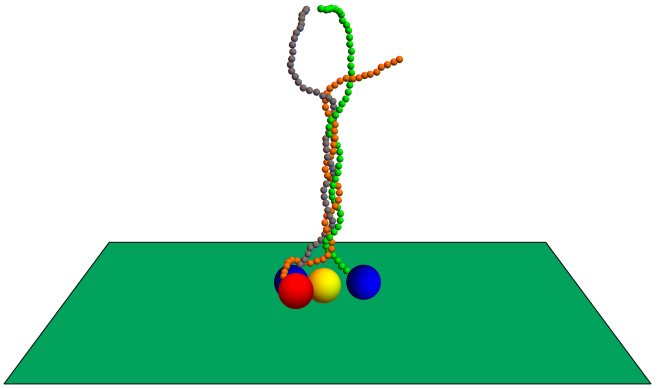

Movie S1. The simulation shown in Fig. 2 in the main text.

Movie S1

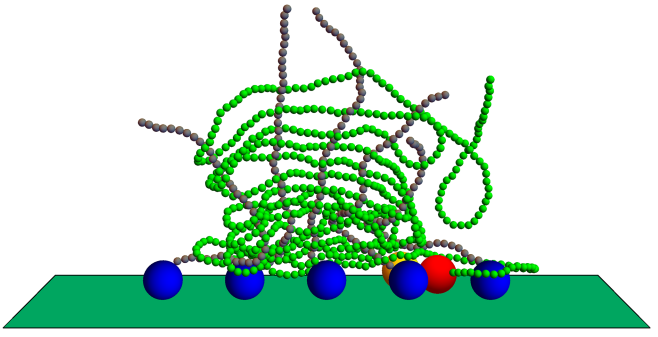

Movie S2. The simulation shown in Fig. 3 in the main text.

Movie S2

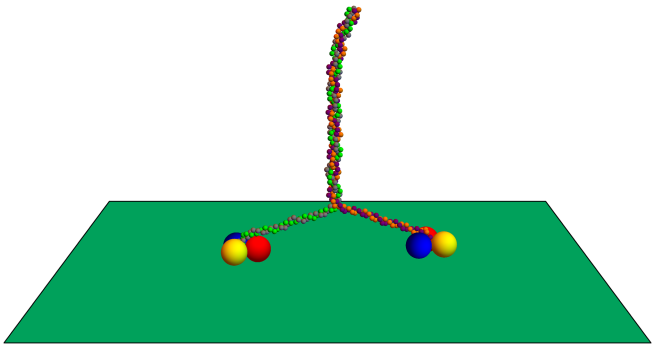

Movie S3. The simulation shown in Fig. 4 in the main text.

Movie S3